Радіофізика і радіоастрономія. 2020, Т. 25, № 4, с. 308–323

DOI: https://doi.org/10.15407/rpra25.04.308

V. H. KOMENDANT

Observatory "URAN-4", Institute of Radio Astronomy,
National Academy of Sciences of Ukraine,
1v, Marazliivska St., Astronomical Observatory, Odesa, 65014, Ukraine
E–mail: votan1360@gmail.com

# ON THE CHARACTER OF AN ARTIFICIAL SATELLITE DRAG UNDER VARIOUS STATES OF SOLAR AND GEOMAGNETIC ACTIVITY

Purpose: *The artificial satellites drag in the atmosphere remains an urgent problem to date. In this work, the artificial satellites data are used in order to study the atmosphere state under various manifestations of solar and geomagnetic activity. The selected satelites were moving uncontrollable being good indicators of the upper atmosphere state. The B-star (drag term) drag coefficient is used in this work. This term is used in the SGP and SDP models to take into account the resistance of the atmosphere to the satelite orbital motion. The data of the drag of two artificial satellites, one moving in elliptical and the other in circular orbits at midlatitudes (orbital plane angles of 58° – 60° ) were considered. These data include the end of the 23rd solar activity cycle, as well as the growth, the maximum and the decay phases of the 24th solar cycle (years 2005–2017). Seven periods of anomalous drag of the satellites were analyzed. They are: 4 monthly periods (two in 2005 and two in 2011) and 3 yearly periods (within 19.07.2014 to 22.08.2015), five-year long (2005–2010) and six-year long (2011–2017) periods.*

Design/methodology/approach: *The periodogram analysis was made. This allowed to reveal the periodic processes in changes in the state of the atmosphere of different duration. The correlation coefficients of the B-star drag term with the indices of solar and geomagnetic activity were calculated. The analysis of extreme drag of the satellites in the periods of the increased solar and geomagnetic activity (intervals of observation lasting a month) was made.*

Findings: *Using the solar and geomagnetic data we found that some month-long part of the anomalous drag periods were followed by flares on the Sun and the arrival of the coronal mass ejections into the near-Earth space. At time intervals of year-long observations the highest values (0.5 – 0.7) were obtained for the coefficients of the B-star parameter correlation with the solar activity indices – solar radiation at the wavelength of 10.7 cm, F10.7, and Lyman alpha radiation, $L_\alpha$. At monthly time intervals, the largest values of the correlation coefficients were obtained for the B-stars with the electron fluxes with energies above 0.6 and 2 MeV, E, (0.3 – 0.5), the Lyman alpha radiation, $L_\alpha$, (0.58 – 0.73 for a circular orbit satellite), and the solar constant, TSI, (0.3 – 0.6), as well as the geomagnetic storms intensity index, $D_{st}$, (0.66 – 0.69). Periodogram calculations show the presence of a whole spectrum of periods in the deceleration of a circular orbit satellite and a dedicated period for an elliptical orbit satellite.*

Conclusions: *The B-star drag term dependences on the indices of solar and geomagnetic activity during some periods of their intensification for the 23–24 cycles of solar activity are considered. The periodogram analysis made together with the analysis of the conditions and parameters of space weather allows to see the general and more detailed picture of the solar and geomagnetic activity influence on the change in the motion of the satellite in the atmosphere. The B-star drag term helps to consider only the atmosphere influence on the artificial satellite movement in the near-Earth space.*

Key words: *artificial satellite, atmosphere, artificial satellite drag, solar activity, geomagnetic activity, space weather*

## 1. Introduction

Artificial satellites observations make it possible to determine changes in the upper atmosphere density, the structure of the Earth's gravitational field, etc., based on disturbances in their orbits. Observations of satellites in orbit provide a unique experimental material for analysis of the effect of space weather on the upper atmosphere state. Many papers on the atmospheric density variations based on the data from satellite observations were published after the launch of the first satellite [1, 2]. The solar and geomagnetic activity significantly affects the state and basic parameters of the Earth' upper atmosphere. The influence of solar activity is manifested in two main factors: wave radiation and corpuscular fluxes.

The effect of wave radiation is described in [3–11]. The ideas about the daily and semiannual changes in the atmosphere density, the changes caused by solar and geomagnetic activity are given in [3–6]. The daily changes in the upper atmosphere state can be caused by joint heating of the atmosphere, by UV and corpuscular radiation [4], only by UV radiation [5], only by ion drift [6], by UV radiation and solar radiation in the radio wavelength range [3]. In Jacchia [7] and Roemer [8] works it was noted that the time delays between density changes and indices of solar and geomagnetic activity were found (in 1967) [7]. These delays have different values for the illuminated and unlit hemispheres [8]. The dependence of the atmospheric temperature on changes in the radio flux

within the frequency range of 1000–3750 MHz [11], reflecting the conditions of ionization, was studied. The changes in the radio flux are correlated with the long-term changes in atmospheric temperature were determined.

The effects of the drag of satellites at different altitudes were considered in those years. As a result, the atmospheric drag has the greatest effect on the satellite movement at altitudes up to 700 km; and the solar radiation pressure at altitudes above 700 km were obtained. The influence of these effects increases with the increase in solar activity [9]. The reviews of many factors, which change the state and composition of the atmosphere: space weather, solar ultraviolet radiation, coronal mass ejections (CMEs), had been published [10].

The influence of corpuscular flows is described in works [3, 4, 10–14]. The influence of this component of solar activity was also considered in most of the aforesaid works [3, 4]. Cole considered the indirect influence of solar activity (heating by auroral electric jets) on semiannual changes in atmospheric density in his work [12] in 1971. Illés-Almár [13] showed that in the equatorial region of the neutral upper atmosphere there is a heat source, in addition to corpuscular radiation, which acts during and after geomagnetic storms (in 2004). Paper [11] provides an overview of the factors of geomagnetic heating of the atmosphere, such as injection of charged particles and electrons, magnetohydrodynamic waves and plasma oscillations. CMEs as one of the factors affecting the state of the atmosphere are considered in [10].

Investigations of the upper atmosphere density dependence on geomagnetic storms are based on the data of satellites drag observations.

The irregular density fluctuations, which occur during geomagnetically quiet periods and correlate with small variations in the average planetary geomagnetic index $K_p$, were revealed by Slowey [15]. The delay of the atmosphere response to geomagnetic disturbances, which magnitude depends on the latitude, was found based on the data of the drag of four satellites [16]. The influence of solar activity, which leads to magnetic storms, causing an increase in the atmosphere density and temperature, is considered in [9]. Analysis of the data on the atmospheric density (at altitudes from 160 to 190 km) [17] shows that two strong geomagnetic storms (components $H$ and $Z > 200$ nT), November 1, 1968 and May 15, 1969, were accompanied by density increase by 30 and 70 %, respectively.

The value of the atmospheric density at an altitude of 310 km for midlatitudes was obtained from the Ariel 2 satellite rotation speed recordings [18, 19] in March and April 1964. The fact that the density is closely related to the change in the equatorial $D_{st}$ index was established from the analysis of the atmospheric density, the $D_{st}$ index, and the planetary daily average geomagnetic $A_p$ index.

These studies determine the relationship of the solar activity centers with the interplanetary magnetic field and geomagnetic activity. The influence of the structure of the interplanetary magnetic sector on the Earth is produced on the magnetosphere from the solar side is shown in work [20] in 1972.

In this work, the artificial Earth satellites (AES) are used as indicators of the impact of space weather on the upper atmosphere of the Earth [21, 22].

## 2. Data Used

The data on the extreme deceleration periods of two midlatitude satellites with close orbital inclinations were used for the analysis. These satellites were moving in circular (00397) and elliptical (00746) orbits in an uncontrolled mode. The elements of the satellite 00397 orbit: $i = 58.3°$, $e = 0.0016$, $r_{\min} = 613$ km, $r_{\max} = 621$ km; and those of the satellite 00746: $i = 60.8°$, $e = 0.31$, $r_{\min} = 399$ km, $r_{\max} = 6409$ km. Here $i$ is the inclination of the orbit, $e$ is the eccentricity of the orbit, $r_{\min}$ and $r_{\max}$ are the minimum and maximum distances from the Earth's surface.

The satellites were observed during the end of the 23rd solar cycle period (2005–2008) and almost the entire 24th cycle period (2009–2017). The studies of the 24th cycle included the growth phase, the maximum and the decline phases (Fig. 1).

The models predicting changes in the atmospheric parameters, based on the data of the drag of artificial satellites, and the physical processes determining the dynamics of their movement, were built. The SGP (Simplified General Perturbations) and SDP (Simplified Deep Space Perturbations) models are widely used owing to the TLE (Two-Line Element) set format. The TLE set format, being developed by the NORAD (North American Aerospace Defense Command), is a two-line data format, which represents a set of orbital elements for an Earth satellite [23].

The B-star drag coefficient (drag term) is used in this work. This coefficient is used in the SGP

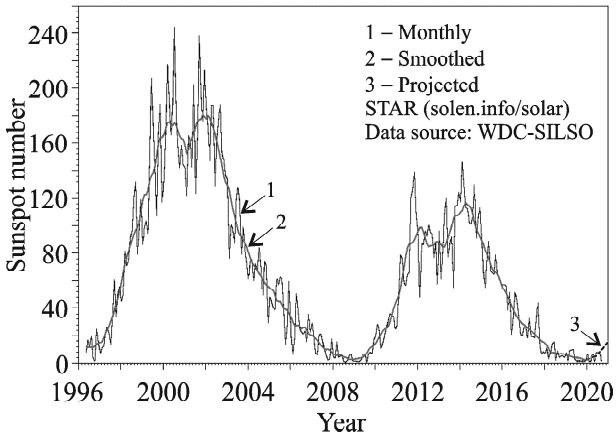


***Fig. 1.*** Monthly sunspot numbers, which illustrate the 23–24 solar activity cycles (Available from: https://www.solen.info/solar/)

and SDP models to take into account the atmospheric drag on the satellite motion and illustrates the satellite's susceptibility to atmospheric drag in orbit [23].

SGP models are applied to objects near the Earth with orbital periods of less than 225 min. These models take into account the influence of perturbations caused by the shape of the Earth, the resistance of the atmosphere and radiation from the Sun [24, 25]. The SDP models are applied to objects with orbital periods greater than 225 min that corresponds to the altitude of 5877.5 km, assuming a circular orbit. These models take into account the gravitational perturbations caused by some other objects such as the Sun and the Moon [24, 25].

In these models the ballistic coefficient is calculated by the formula

$$B = \frac{C_D A}{m},$$

where $B$ is the ballistic coefficient, $C_D$ is the aerodynamic drag coefficient (if the mean free path of air molecules is much larger than the geometric size of the satellite, then $C_D$ is close to 2), $A$ is the midsection area (cross-sectional area of the satellite), $m$ is the satellite mass.

The B-star drag term coefficient is related to the ballistic coefficient by the formula

$$B^* = B\frac{\rho_0}{2},$$

where $B^*$ is the modified ballistic coefficient or B-star drag term, $\rho_0$ is some standard density value for a given altitude. The B-star drag term coefficient has the dimension of $1/R_E$, where $R_E = 6371$ km is the radius of the Earth.

A number of difficulties arise, some of which are associated with calculating the atmospheric wind speed perpendicular to the cross-sectional area of the satellite, and the impossibility of accurately taking into account the $C_D$ parameter. Thus, all models, when estimating the $B$ parameter, correct it so that the calculated parameters correspond to the observed positions of the object in the best way. For this reason, this work uses just this coefficient.

## 3. Analysis of the Dynamics of Extreme Drag of Satellites at Various States of Solar and Geomagnetic Activity

Two satellites moving in the circular and in the elliptical orbits were taken for analysis. The changes in the drag coefficient for the satellite 00397 moving in the circular orbit and the satellite 00746 moving in the elliptical orbit over the entire research period are shown in Figs. 2 and 3.

### 3.1. On the Satellite Drag for the Period of the 23rd and 24th Solar Activity Cycles of 2005−2017

The data in this work cover the decline phase of the 23rd cycle (2005–2008), the growth, maximum and decline phases of the 24th cycle (2009–2017). To consider various conditions affecting the drag nature of satellites, this is very important. The B-star drag coefficient for the two selected satellites during the decline phase of the 23rd solar cycle and two years of the growth phase of the 24th solar cycle (2005–2010) is shown in Figs. 4 and 5.

The state of the Earth's upper atmosphere is influenced by the solar activity, or rather the wave and corpuscular components of the solar radiation. These components of wave and corpuscular radiation affect the change in the state and density of the upper atmosphere. They depend, first of all, on the flux of radio emission from the Sun at the wavelength of 10.7 cm (as the index of ultraviolet radiation from the Sun) and geomagnetic disturbances. In addition, in this work a wide range of indices reflecting the state of space weather are used: $W$ – the Wolf number, $S_p$ – the total area of the sunspots, $F10.7$ – the radio emission from the Sun at the wavelength of 10.7 cm,

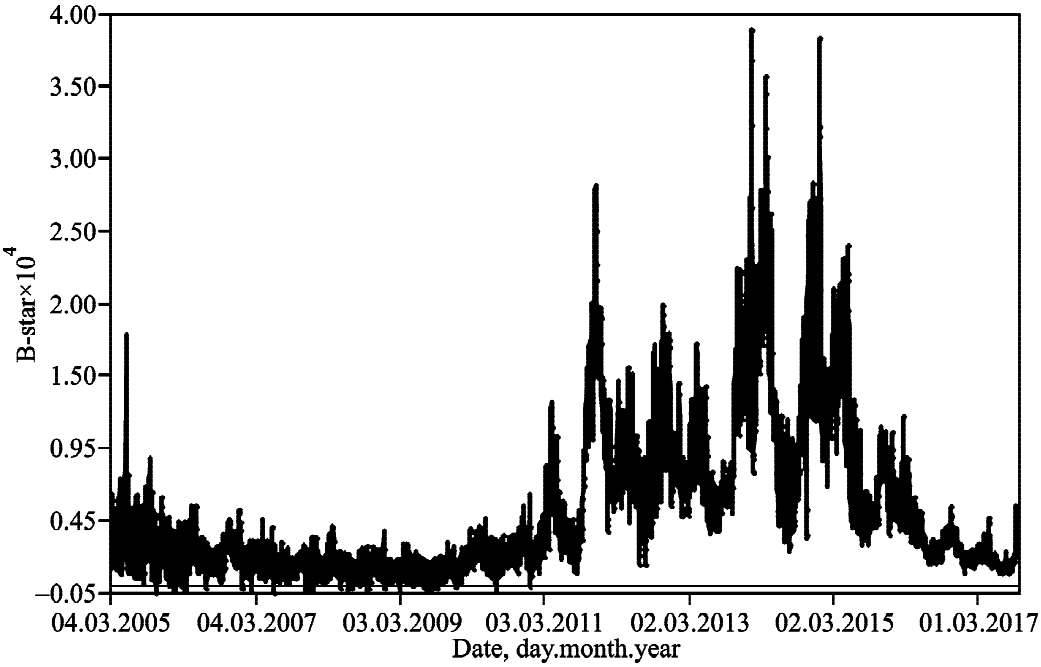


***Fig. 2.*** Change of the B-star coefficient for the satellite 00397 moving in the circular orbit; $i = 58.3°$

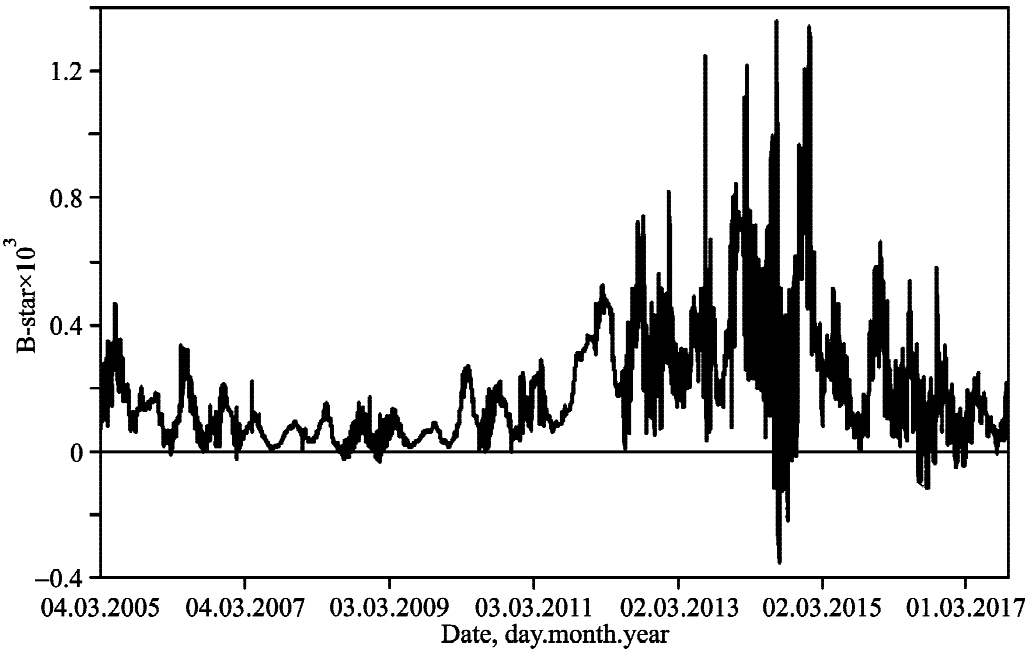


***Fig. 3.*** Change of the B-star coefficient for the satellite 00746 moving in the elliptical orbit; $i = 60.8°$

*TSI* – the solar constant, $L_\alpha$ – the Lyman alpha radiation, *E* – the fluxes of electrons with energies greater than 0.6 MeV and 2 MeV, the solar wind parameters, *IMF* – the interplanetary magnetic field, $A_p$ – the planetary geomagnetic index, $D_{st}$ (Disturbance Storm Time Index) – the index of the intensity of geomagnetic storms.

The Wolf number, *W*, and the total area of the sunspots, $S_p$, (characterize the general course of the 11-year cycle of solar activity.

The *F*10.7, *TSI* and $L_\alpha$ indices characterize the wave component of the solar radiation.

The radio emission from the Sun at the wavelength of 10.7 cm, *F*10.7, characterizes the wave

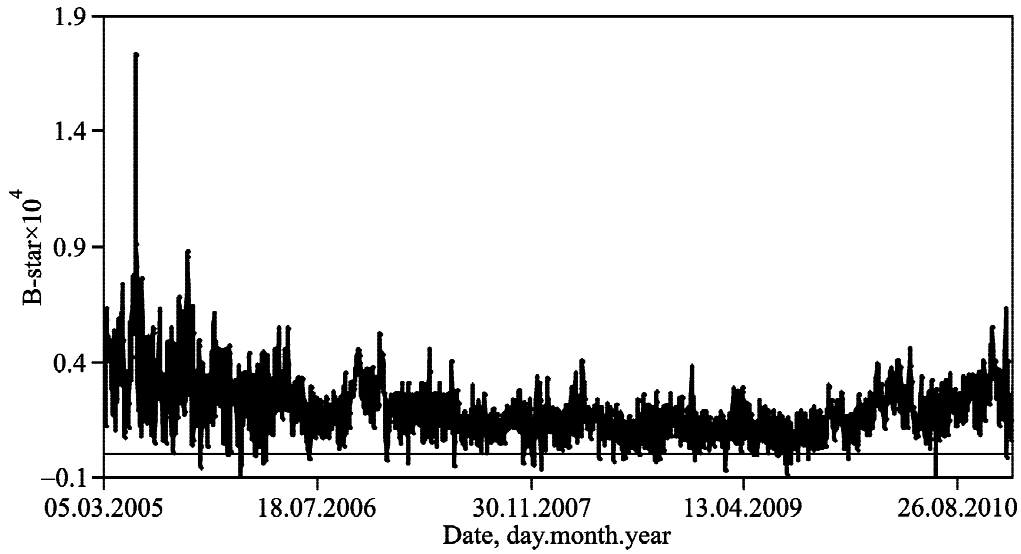


***Fig. 4.*** Changes in the B-star coefficient for the circular orbit satellite 00397 over the period of 2005–2010; $i = 58.3°$

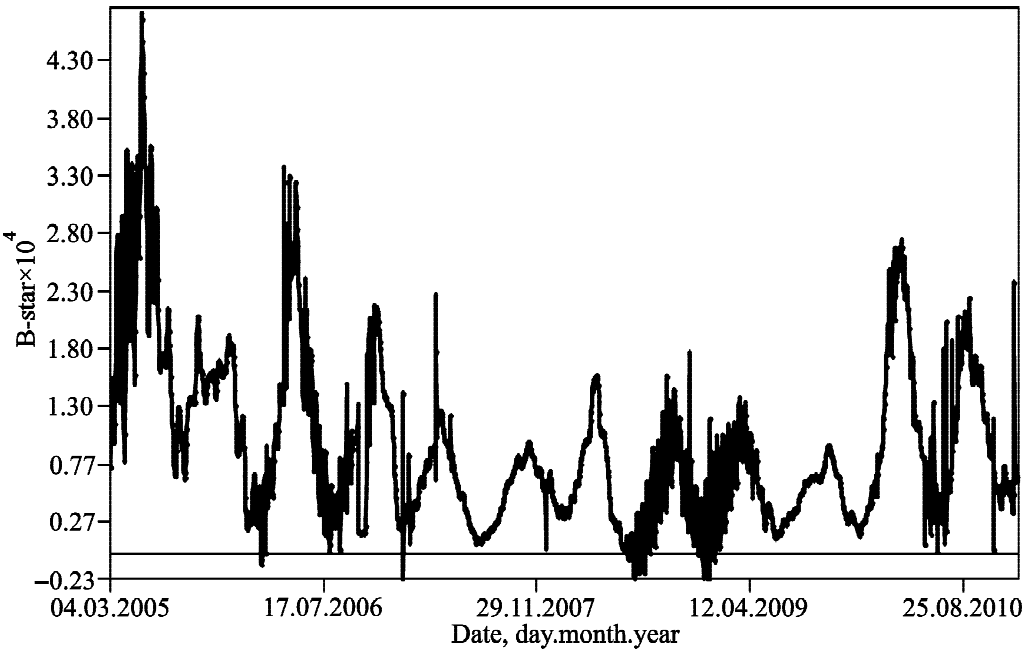


***Fig. 5.*** Changes in the B-star coefficient for the elliptical orbit satellite 00746 over the period of 2005–2010; $i = 60.8°$

flux, which correlates with the ultraviolet and the X-ray fluxes of the Sun.

The solar constant, *TSI*, is a measure of the amount of solar energy received by a body located at a cetain distance from the Sun. For the Earth, *TSI* is defined as the solar energy received per unit area in the upper atmosphere with an average distance from the Earth to the Sun equal to 1 AU. The *TSI* is approximately 1.35 mW/cm$^2$. This "constant" changes every day, as does sunspot activity, and over longer periods of time depending on the solar cycle.

The Lyman alpha radiation, $L_\alpha$, is a spectral series in the spectrum of the hydrogen atom, was named after the physicist Theodore Lyman, who discovered this series in 1906. The series is formed during transitions of electrons from the high energy levels to the first one in the emission spectrum and from the first level to all others during absorption. At normal con-

ditions, $L_\alpha$ is located in the ultraviolet region of the spectrum.

The electron fluxes with energies greater than 0.6 MeV and 2 MeV, $E$, and the solar wind parameters reflect the corpuscular component of the Sun's activity. They reflect the effect on ionospheric currents, which forms the magnetosphere.

The indices $IMF$, $A_p$, and $D_{st}$ show the disturbance of the interplanetary environment, the magnetosphere reaction to changes in the conditions in the interplanetary environment, and the intensity of disturbances in the magnetosphere, respectively.

The interplanetary magnetic field, $IMF$, is a component of the solar magnetic field, which is pulled from the solar corona by the flow of the solar wind and fills the solar system.

The planetary geomagnetic index, $A_p$, characterizes the degree of the solar activity effect on the magnetosphere.

To analyze the magnetic storms, the $D_{st}$ index is used. It is an axisymmetric component of the perturbed magnetic field with respect to the geomagnetic dipole and is determined on the basis of magnetic field measurements at four near-equatorial stations: San Juan, Hermanus, Kakioka, Honolulu.

To determine the full spectrum of periods available in the studied observation interval (2005–2010) and to estimate their amplitudes and power, the periodograms were built. The periodograms for the drag coefficient of two satellites are shown in Figs. 6 and 7. Figs. 8–11 show the periodograms of the solar and geomagnetic activity indices, which have the highest correlation coefficients with the B-star: $L_\alpha$ $(0.57-0.61)$, $F10.7$ $(0.54-0.56)$, $S_p$ $(0.44-0.46)$, $W$ $(0.5-0.51)$.

The periodograms for the satellites drag (Figs. 6 and 7) show a significant difference in the presence of periods and the ratio of their amplitudes for the circular orbit satellite and the elliptical orbit satellite. A circular orbit satellite has a wide range of periods of various amplitudes with a predominance periods of 5.8 months ($7.3\cdot10^{-9}$) and 10.6 days ($7.8\cdot10^{-9}$). At the same time, for the elliptical orbit satellite, the only one period shows predominance and it is 5.8 months ($2.6\cdot10^{-6}$).

As a result, for the satellite 00397, moving in the circular orbit, the periods of (in descending order of the periodogram and spectral density) 10.6 days ($7.8\cdot10^{-9}$), 5.8 months ($7.3\cdot10^{-9}$), 1.6 year ($4.5\cdot10^{-9}$), 26.3 days ($3.7\cdot10^{-9}$), 3.9 months ($2.7\cdot10^{-9}$), and 2.1 months ($2.3\cdot10^{-9}$) were found.

For the satellite 00746, moving in the elliptical orbit, the periods (in descending order of the periodogram and spectral density) of 5.8 months ($2.6\cdot10^{-6}$), 11.8 months ($2.5\cdot10^{-7}$), 3.9 months ($2\cdot10^{-7}$), 2.4 months ($5.3\cdot10^{-8}$), and 12.7 days ($4.2\cdot10^{-8}$) were found. All the aforesaid periods, based on the calculations of the correlation coefficients between the B-star and the indices of solar and geomagnetic activity, are caused by changes in the indices of the wave radiation of the Sun – $F10.7$ and $L_\alpha$. For the circular orbit satellite, the correlation coefficient of the B-star with the index $F10.7$ makes 0.56 and with the index $L_\alpha$ – 0.61. For the elliptical orbit satellite the correlation coefficient of the B-star with the index $F10.7$ makes 0.54 and with the index $L_\alpha$ – 0.57. All of these

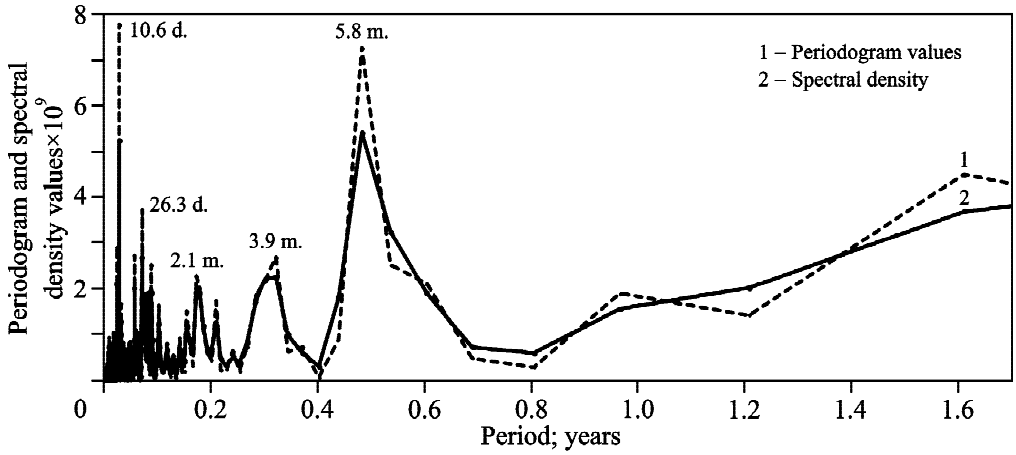


***Fig. 6.*** Periodogram for the B-star coefficient of the circular orbit satellite 00397 (2005–2010); $i = 58.3°$

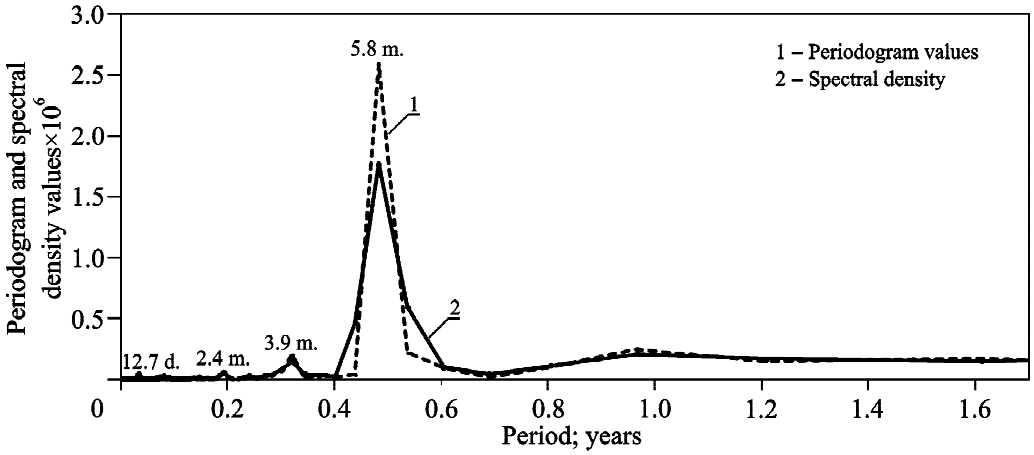


***Fig. 7.*** Periodogram for the B-star coefficient of the elliptical orbit satellite 00746 (2005–2010); $i = 60.8°$

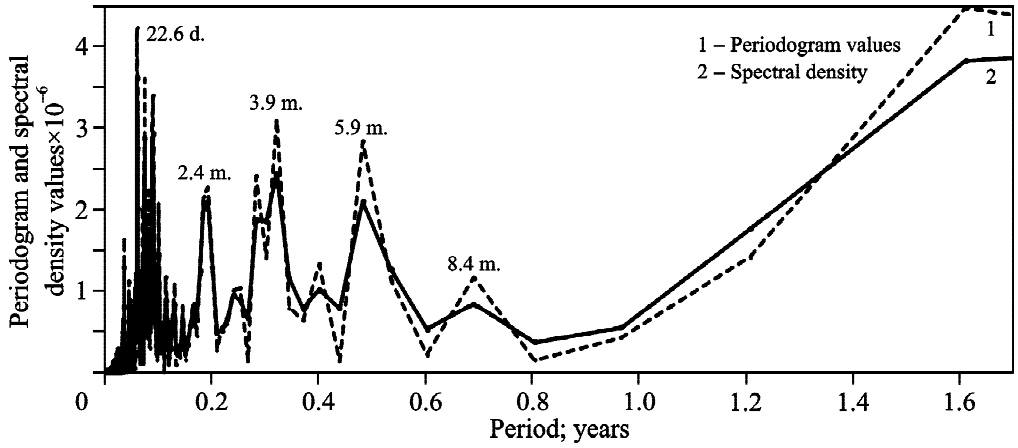


***Fig. 8.*** Periodogram for the total sunspot area $S_p$ (2005–2010)

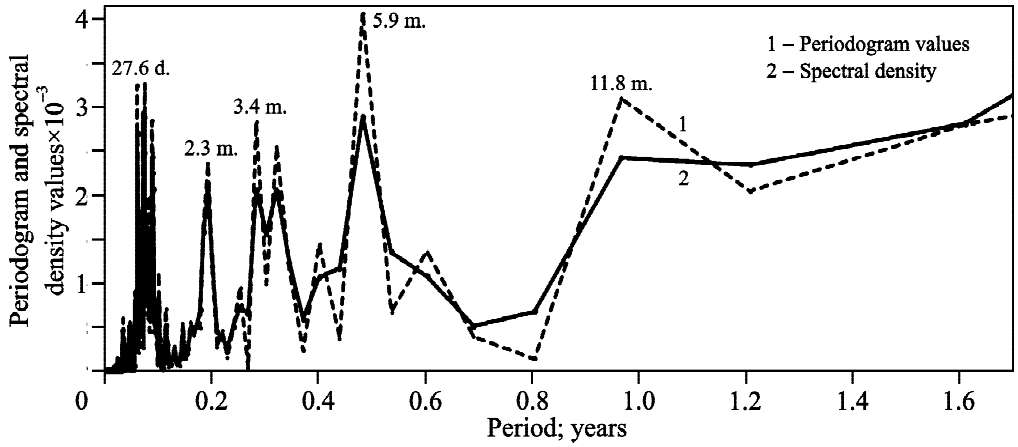


***Fig. 9.*** Periodogram for the $F10.7$ solar flux index (2005–2010)

indices have the period of 5.8 months. Periods of 3.9 months, 12.7 days, 10.6 days are found in the $A_p$, and $D_{st}$ indices and may be associated with their variations.

The B-star coefficient change during the growth, maximum and decline phases of the 24th solar cycle of 2011–2017 for the two satellites is shown in Figs. 12 and 13.

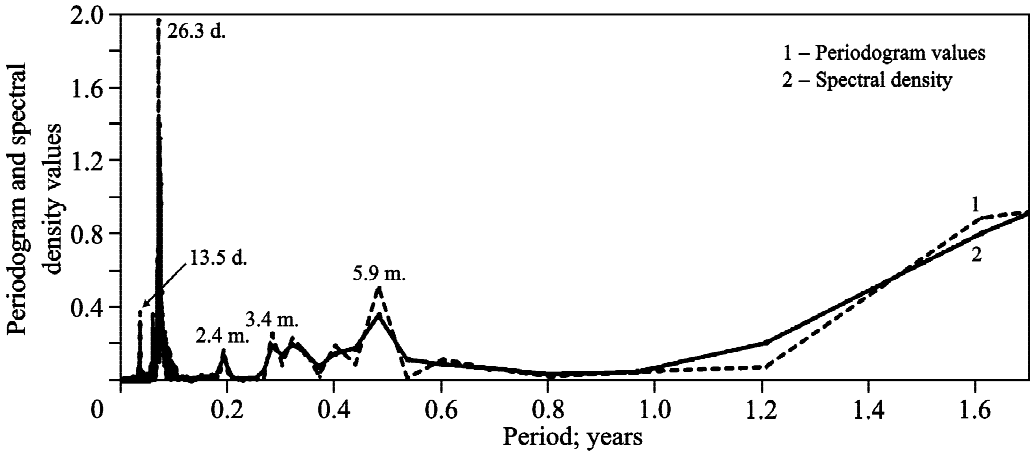


***Fig. 10.*** Periodogram for the Lyman alpha radiation index $L_\alpha$ (2005–2010)

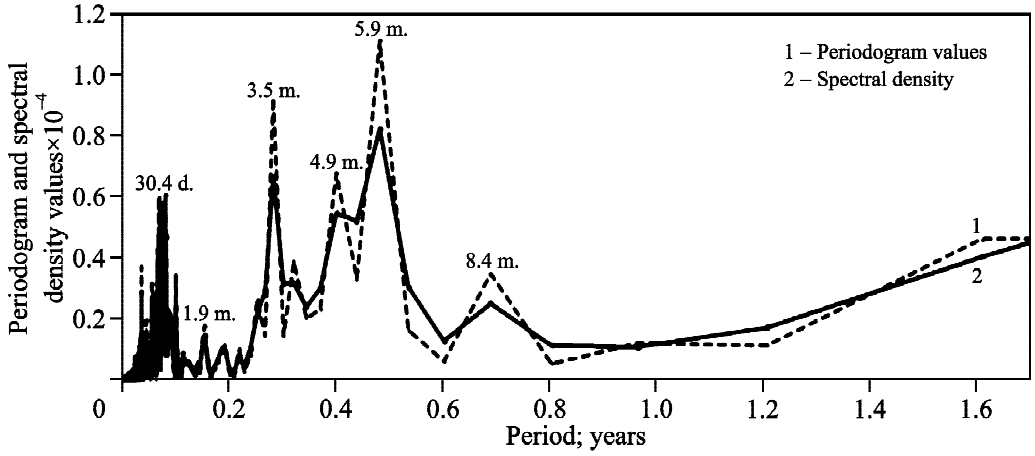


***Fig. 11.*** Periodogram for the Wolf number $W$ (2005–2010)

For the satellite 00397 moving in the circular orbit at the time interval of 2011–2017, the periods of (in descending order of the periodogram and spectral density) 1.1 year ($7.2\cdot10^{-7}$), 6.2 months ($3.3\cdot10^{-7}$), 9.3 months ($2.1\cdot10^{-7}$), 26 days ($1.2\cdot10^{-7}$) 1.3 months ($9.9\cdot10^{-8}$), and 4.1 months ($9.7\cdot10^{-8}$) were found. The predominant periods for the circular orbit satellite are the periods of 1.1 years ($7.2\cdot10^{-7}$) and 6.2 months ($3.3\cdot10^{-7}$). We have found that from the periodograms being built for the time interval of 2011–2017. It will also be observed that for the periods for the circular orbit satellite at the growth, maximum and decline phases of the 24th solar cycle, the periodogram and spectral density values increased in 2 orders of magnitude as compared with the decline phase of the 23rd solar cycle.

For the satellite 00746, moving in the elliptical orbit, the following periods of (in descending order of the periodogram and spectral density) 5.8 months ($1.2\cdot10^{-5}$), 11.7 months ($6.1\cdot10^{-6}$), 9.4 months ($3.6\cdot10^{-6}$), 4.7 months ($2.4\cdot10^{-6}$), 22.7 days ($6.8\cdot10^{-7}$), and 1.2 months ($5\cdot10^{-7}$) were found at the time interval of 2011–2017. For the satellite moving in the elliptical orbit, the predominant periods are 5.8 months ($1.2\cdot10^{-5}$) and 11.7 months ($6.1\cdot10^{-6}$).

The periodogram and spectral density for the period of 5.8 months increased by an order of magnitude as compared to the period of 2005–2010 (decline phase of the 23rd solar cycle) for the elliptical orbit satellite. The change in the amplitudes indicate a transition to a different cycle of solar activity that results in the solar activity increase.

Based on the calculations of the coefficients of correlation between the B-star drag term and the indices of solar and geomagnetic activity, the periods for the observation interval of 2011–2017 are also

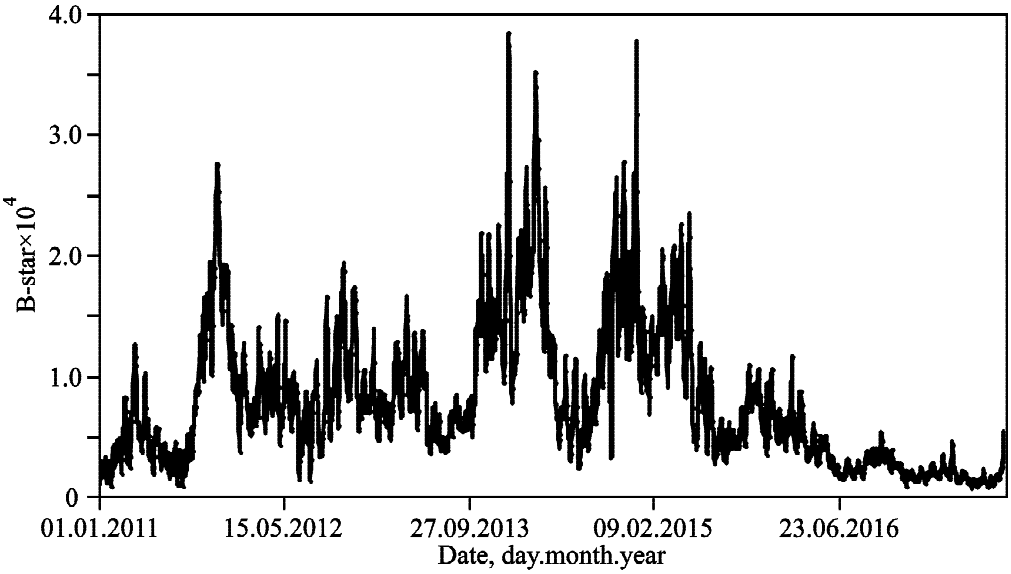


***Fig. 12.*** Changes in the B-star coefficient for the circular orbit satellite 00397 over the 2011–2017 period; $i = 58.3°$

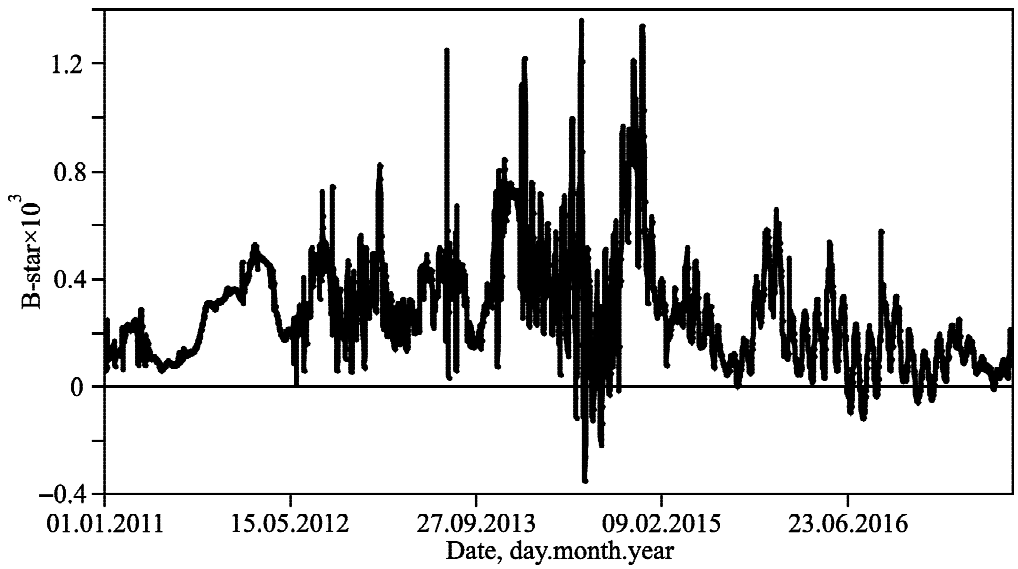


***Fig. 13.*** Changes in the B-star coefficient for the elliptical orbit satellite 00746 over the 2011–2017 period; $i = 60.8°$

caused by changes in the indices of the solar wave radiation – $F10.7$ and $L_\alpha$. For the circular orbit satellite, the correlation coefficient of the B-star with the index $F10.7$ makes 0.81 and with the index $L_\alpha$ – 0.82. For the elliptical orbit satellite, the correlation coefficient of the B-star with the index $F10.7$ makes 0.66 and with the index $L_\alpha$ – 0.64.

The cycle change process have also an effect on the values of the correlation coefficients between the B-star and the indices of solar and geomagnetic activity. The correlation coefficients between the B-star and the indices, which describe the wave component of solar activity and the general activity cycle, for the 2011–2017 increase as against the correlation coefficients in 2005–2010 for both satellites.

The periods (at the 2011–2017 observation interval) of 9.5 months, 11.7 months and 1.1 year are added to the periods determined for 2005–2010. They can be seen in Figs. 12 and 13 in the form of large and long maxima. The similar maximum of the satellite drag change with the period of 1.1 year (July 19, 2014 – August 22, 2015) is shown in Fig. 14 in more detail.

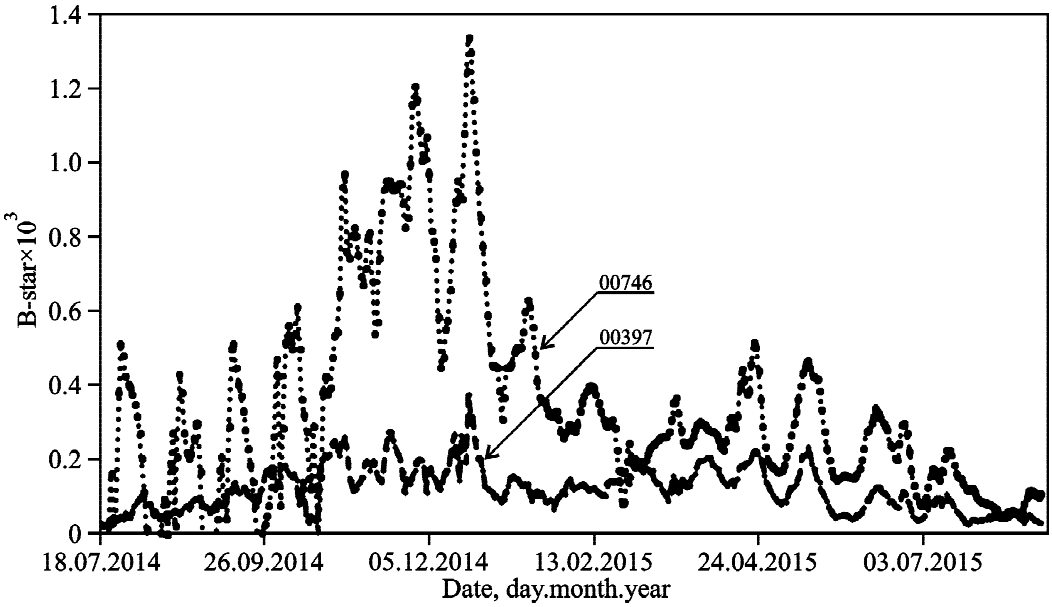


***Fig. 14.*** Changes in the B-star coefficient for the circular orbit satellite 00397 and the elliptical orbit satellite 00746 at the period from July 19, 2014 to August 22, 2015

For the aforesaid yearly period (19.07.2014 – 22.08.2015), the highest values of the B-star correlation coefficients were obtained with the following indices: $L_\alpha$ (0.52 – 0.68), $F10.7$ (0.59 – 0.66), and $S_p$ (0.44). The following periods of 25 days ($9.7\cdot10^{-8}$), 20 days ($8.5\cdot10^{-8}$), 1.3 months ($2\cdot10^{-8}$), 1.9 months ($1.8\cdot10^{-8}$), 10.8 days ($1.1\cdot10^{-8}$), 14 days ($8\cdot10^{-9}$), and 8.8 days ($7.6\cdot10^{-9}$) were found from the periodograms of the circular orbit satellite 00397. The predominant periods for the studied observation interval (July 19, 2014 – August 22, 2015) are 25 days ($9.7\cdot10^{-8}$) and 20 days ($8.5\cdot10^{-8}$). Periods of 1.9 and 1.3 months can be caused by the change in the $S_p$ index (the similar period was not found for the $L_\alpha$ and $F10.7$ indices).

The periods of 6.7 months ($9.4\cdot10^{-6}$), 25 days ($1.7\cdot10^{-6}$), 10.8 days ($7.6\cdot10^{-8}$), and 8 days ($5.9\cdot10^{-8}$) were found for the elliptical orbit satellite 00746. The first two periods are not present in the $F10.7$ index. The predominant periods: 6.7 months ($9.4\cdot10^{-6}$) and 25 days ($1.7\cdot10^{-6}$) – for the studied observation interval (July 19, 2014 – August 22, 2015). The period of 6.7 months is caused by the change in the $S_p$ index and is also present in it; the period of 25 days is caused by the change in the $L_\alpha$ index. A period of 26 days is found in the $L_\alpha$ index.

We have analyzed 4 events, with maximum amplitudes of the B-star index, at extreme events in the 23–24 solar activity cycles, described below.

### 3.2. On the Nature and Causes of the Satellite Drag During the End of the 23rd Cycle of Solar and Geomagnetic Activity in May 2005

The beginning and the maximum of the given event are different for each satellite. For the circular orbit AES 00397, the disturbance caused by the drag in the upper atmosphere began to increase on May 15, having reached the maximum on May 17, and decreased on May 19–22 (with the drag increases on May 3, 6, 10, 14, 17, and 24).

The normalized graphs of changes in the B-star index and indices of solar and geomagnetic activity with the highest correlation coefficients from 0.45 to 0.6 are shown in Figs. 15 and 16.

One of the reasons for the change in the motion of the "circular" satellite is the flow of electrons as the graphs in Figs. 15 and 16 show. Also, the upper atmosphere disturbance was caused initially by a high-speed flow of the solar wind from the coronal hole directed towards the Earth from May 6 to 7, and was being supported by radiation from the M-class flares and the CMEs (which reached the near-Earth space) associated with them (2, 11, 13 and 16 May) in this period. The effect of wave emission from the M-class flares can be seen as three small peaks with the maxima on May 6, 10 and 13–14 on the graph for the circular orbit satel-

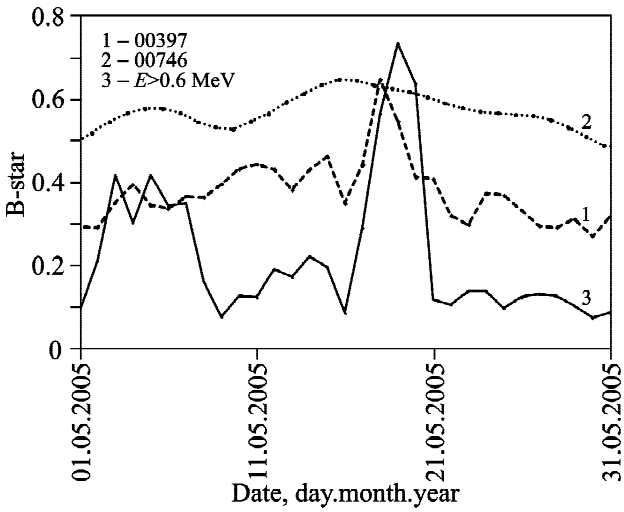


***Fig. 15.*** Changes in the B-star index for the circular orbit satellite 00397 and the elliptical orbit satellite 00746, the electron flux with energies greater than 0.6 MeV ($E > 0.6$ MeV) for May 2005

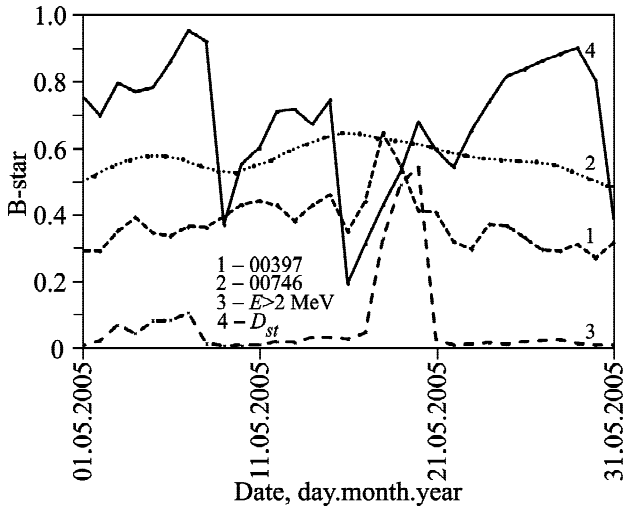


***Fig. 16.*** Changes in the B-star index for the circular orbit satellite 00397 and the elliptical orbit satellite 00746, the electron flux with energies greater than 2 MeV ($E > 2$ MeV), the geomagnetic storm intensity index ($D_{st}$) for May 2005

lite 00397 (Fig. 15). On the said dates, the M-class flares were recorded.

Perturbation of the motion of the AES 00746 moving in the elliptical orbit manifested itself weakly starting on May 9, having maximum on May 15 and decline on May 30.

Manifestations of the solar activity (mentioned above) caused two strong (strong $K_p = 5-7$, $G = 3$) magnetic storms with a sudden onset on May 7–9 and on May 15–16, and increased geomagnetic disturbance at high latitudes that coincides with the beginning and maximum of an increase in a satellite drag in the elliptical orbit. The satellites did not react upon the most probable shock waves (May 15 and 29) associated with the CME from the M-class flares on May 13 and 26 as can be seen in Figs. 15 and 16.

The maximum of the B-star index of the elliptical orbit satellite 00746 on May 15 coincides with a sharp increase in the speed and density of the solar wind flux, according to the SOHO space observatory data. The drag increase on May 3, 6, 10, 14, 17, and 24 for the circular orbit satellite 00397 coincides with an insignificant increase in density and speed of the solar wind.

## 3.3. On the Nature and Causes of the Satellite Drag During the End of the 23rd Cycle of Solar and Geomagnetic Activity in September 2005

The beginning and the maximum of the September event for the satellite 00397 (in the circular orbit) occurred on September 11–15. The event ended on September 25 and includes two maxima on September 20 and 23.

The normalized graph of the change in the B-star index and the indices of solar and geomagnetic activity with the highest correlation coefficients from 0.5 to 0.6 are shown in Fig. 17.

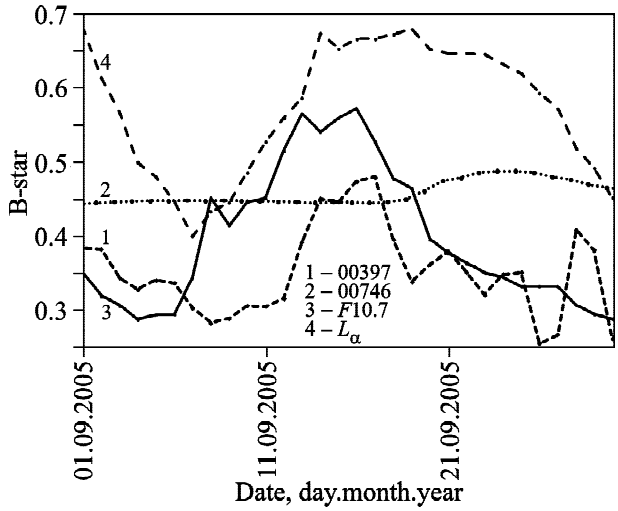


***Fig. 17.*** Changes in the B-star index for the circular orbit satellite 00397 and the elliptical orbit satellite 00746, the solar radio flux at the wavelength of 10.7 cm ($F10.7$), the Lyman alpha radiation ($L_\alpha$) for September 2005

The increase in the atmospheric drag in this time period for the AES 00397 (in the circular orbit) can be associated with high flare activity: the M-class flares (14 events) and the X-class flares (7 events) were observed on September 6–12 and the CME, which came in the near-Earth space and caused strong disturbances in the Earth's magnetic field on September 9–11. The increase in the drag of the satellite 00397 on September 15 coincides with the CME–associated shock wave caused by the X-class flare on September 13, according to the SOHO data.

The satellite moving in the circular orbit did not react to a severe (severe $K_p = 7-8,\ G = 4$) geomagnetic storm on September 9–12, in contrast to an extremely strong (extreme $K_p = 8-9,\ G = 5$) magnetic storm with gradual beginning on September 12–13.

The most powerful flare for the entire 23rd solar cycle, X17, was recorded on September 7. Both satellites did not react to this event, since it occurred on the eastern limb of the Sun and was not directed towards the Earth (Fig. 17).

At the same time, the most noticeable was the drag of the circular orbit satellite 00397 in the period from September 20 (in the form of a long-term trend) till September 30. These drag's peaks are not reflected in the SOHO data on solar wind density and speed. The elliptical orbit satellite 00746 did not experience disturbances, as it can be seen in Fig. 17.

### 3.4. On the Nature and Causes of the Satellite Drag During the 24th Cycle of Solar and Geomagnetic Activity in April 2011

For the satellite 00397 (in the circular orbit) this event began on March 30 with the maximum on April 6 and the end on April 13 (Fig. 18).

The normalized graph of the change in the B-star index and the indices of solar and geomagnetic activity with the highest correlation coefficients from 0.58 to 0.6 are shown in Fig. 18. The correlation coefficients of the indices of solar and geomagnetic activity with the B-star values for the satellite 00746 do not exceed 0.3. The wave radiation of the Sun is a possible factor affecting the change in the movement of satellites during this period (Fig. 18).

The B-class (30 events) and C-class (32 events) flares were observed during this period. They were associated with the CMEs, one of which could be geoeffective. The CME (speed 650 km/s) directed

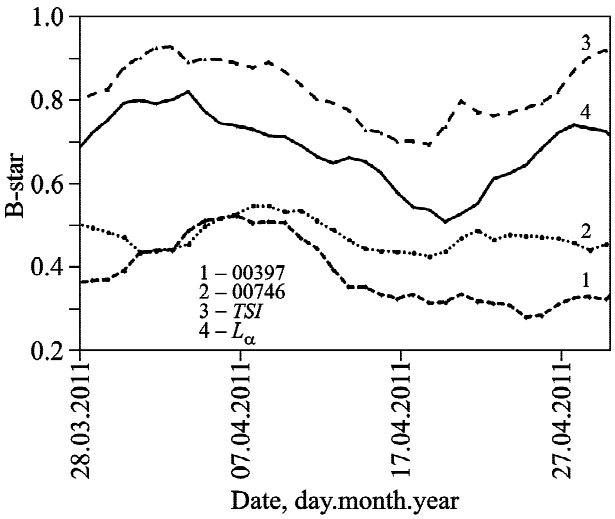


***Fig. 18.*** Changes in the B-star index for the circular orbit satellite 00397 and the elliptical orbit satellite 00746, the solar constant (*TSI*), the Lyman alpha radiation ($L_\alpha$) for April 2011

southwards of the ecliptic plane, which could affect the Earth, was recorded on April 3.

This period of the drag of the satellites can be associated with geomagnetic disturbances caused by the coronal hole, flare activity, and solar wind fluxes.

The minor geomagnetic disturbance (minor $K_p = 5,\ G = 1$) was recorded on April 1–4. It was caused by the flux of energetic particles from the solar coronal hole. Sudden geomagnetic disturbances were recorded on March 29 and 30.

This drag period began on March 31, reached the maximum on April 7, and ended on April 14 for the satellite 00746 (in the elliptical orbit). During this period, moderate (moderate $K_p = 5-6,\ G = 2$) geomagnetic disturbances were recorded on April 6, 12, 13.

The second event with the beginning on April 18 and maximum on April 21 can be seen for the AES 00746 in Fig. 18. Probably, it is related to the CME, which occurred on April 15. The CME reached the Earth, and caused a minor (minor $K_p = 5,\ G = 1$) sudden geomagnetic storm (which is confirmed by the data of geomagnetic disturbance) and the shock wave on April 18. The maximum of the B-star index of the satellite 00746 coincides with a sharp increase in the speed and a slight increase in the solar wind flux density on April 18 according to the SOHO data.

The most probable shock waves were recorded on March 29, April 8 and 18.

The main maximum of the B-star index for the both satellites were accompanied by a sharp increase in the solar wind flow velocity on April 1.

### 3.5. On the Nature and Causes of the Satellite Drag During the 24th Cycle of Solar and Geomagnetic Activity in November 2011

The November event, which began on November 1, is clearly seen only for the AES 00397 moving in the circular orbit, and has a clearly pronounced maximum on November 16, followed by a decline to the minimum on November 28 (Fig. 19).

The normalized graphs of changes in the B-star index and the indices of solar and geomagnetic activity with the highest correlation coefficients 0.44, 0.69 and 0.7 are shown in Figs. 19 and 20.

The change in the B-star index can be associated with the CME produced by the flares of different classes. The CME with the speed of 750 km/s directed towards the Earth was associated with the M-class flare of November 9. The C-class flash produced the CME with the speed of 825 km/s on November 11. It had the trajectory tangent to the Earth.

Strong geomagnetic activity was recorded on November 1 (strong $K_p = 7$, $G = 3$) and the minor one on November 2 (minor $K_p = 5$, $G = 1$) according to [26].

The solar wind speed had slowly increased since November 6 and reached its maximum on November 15, according to the SOHO data.

The C-class (130 events), B-class (12 events), M-class (13 events) flares were observed from November 1 to 27. The X-class flare was observed on November 3. The CMEs, which occurred on November 14–20, did not become geoeffective.

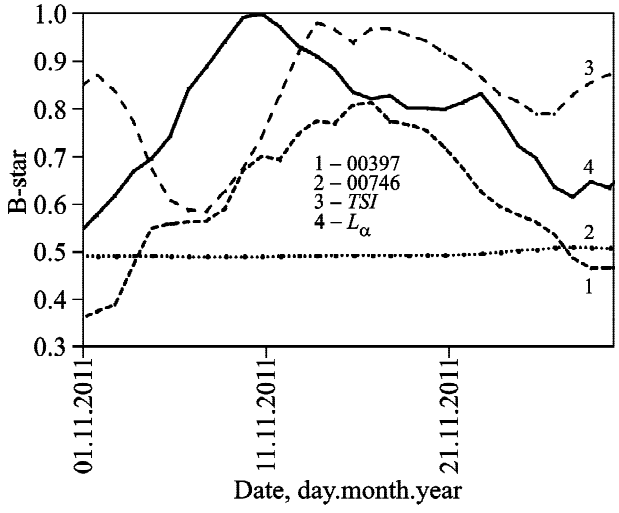


*Fig. 19.* Changes in the B-star index for the circular orbit satellite 00397 and the elliptical orbit satellite 00746, the solar constant (*TSI*), the Lyman alpha radiation ($L_\alpha$) for November 2011

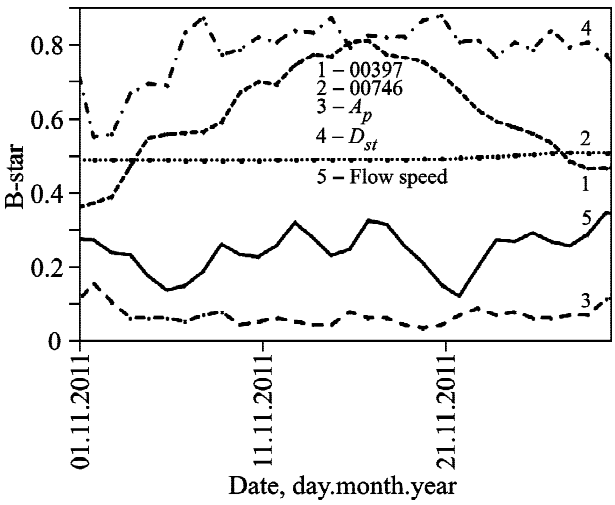


*Fig. 20.* Changes in the B-star index for the circular orbit satellite 00397 and the elliptical orbit satellite 00746, the planetary geomagnetic index ($A_p$), the geomagnetic storm intensity index ($D_{st}$) for November 2011

## 4. Conclusions

The dependences of the B-star drag term on the indices of solar and geomagnetic activity are considered during some isolated periods of their intensification in the 23rd and 24th cycles of solar activity.

The periodogram analysis showed the following features of the presence and changes in quasiperiodic processes of the drag of the satellites:

1. The circular orbit satellite has a wide range of periods of various amplitudes with the predominant periods of 5.8 months ($7.3 \cdot 10^{-9}$) (half a year period), and 10.6 days ($7.8 \cdot 10^{-9}$) during 2005–2010. At the same time, for the elliptical orbit satellite only one predominant period of 5.8 months ($2.6 \cdot 10^{-6}$) can be observed.

2. For the circular orbit satellite there are predominant periods of 1.1 year ($7.2 \cdot 10^{-7}$) and 6.2 months ($3.3 \cdot 10^{-7}$) being obtained from the periodograms at the growth, maximum and decline phases of the 24th solar cycle during 2011–2017. For the satellite moving in the elliptical orbit, the predominant periods are 5.8 months ($1.2 \cdot 10^{-5}$) and 11.7 months ($6.1 \cdot 10^{-6}$).

3. The periods at different time intervals of 2005–2010 and 2011–2017 were found using the periodogram analysis. They are caused by changes in the indices

of the wave radiation of the Sun: the radio flux at the wavelength of 10.7 cm and the Lyman alpha radiation based on the correlation coefficients of B-star with the indices of solar and geomagnetic activity.

4. The correlation coefficients of the B-star with geomagnetic indices do not exceed 0.26 in all considered observation intervals (2005–2010 and 2011–2017). Whereas the B-star correlations with the index of the intensity of geomagnetic storms have negative values for the both satellites, which do not exceed –0.42, during the same observation periods (2005–2010 and 2011–017).

5. It will also be observed that for the circular orbit satellite periods at the growth, the maximum and decline phases of the 24th solar cycle, the value of the periodogram and spectral density increased by 2 orders of magnitude as against the decline phase of the 23rd solar cycle. The periodogram and spectral density for the period of 5.8 months increased by an order of magnitude as against the 2005–2010 period (decline phase of the 23rd solar cycle) for the elliptical orbit satellite.

6. The change in the amplitudes of periodograms and spectral density shows the transition to some other cycle of solar activity that leads to the solar activity increase.

7. The cycle change process also tells on the values of the correlation coefficients of the B-star with the indices of solar and geomagnetic activity. The correlation coefficients of the B-star with the indices, which describe the wave component of solar activity and the general activity cycle, for the 2011–2017 time interval, increase as against the correlation coefficients in 2005–2010 for the both satellites.

The same can be seen on the observation interval of July 19, 2014 – August 22, 2015 i.e. high correlation coefficients of the B-star with the indices of the wave component of solar activity: $L_\alpha$ $(0.52-0.68)$, $F10.7$ $(0.59-0.66)$, $S_p$ $(0.44)$ also present.

The data obtained from the analysis of extreme drag of the satellites during the periods of increased solar and geomagnetic activity (observation intervals of a month) showed the following results:

– The satellites moving in the circular orbits are the most sensitive to changes in space weather conditions.

– The response of each satellite to extreme manifestations of space weather is manifested individually for each satellite depending on the satellite orbit parameters (eccentricity, orbital inclination and perigee altitude).

– The elliptical orbit satellite responded but weakly to the electron fluxes and changes in the intensity of geomagnetic storms index in May 2005. One of the reasons for changes in the circular orbit satellite motion are the electron fluxes. The main contribution to the satellite drag increase was made by the solar coronal hole jet and flare activity.

– The $F10.7$ and $L_\alpha$ indices were the key influencing parameters in September 2005, as well as in May 2005. This month, strong flare activity was recorded (14 events of the M-class and 7 events of the X-class flares). No apparent response to the corpuscular component of solar activity and geomagnetic disturbance was observed.

– The April 2011 event can be associated with geomagnetic disturbances caused by the coronal hole, flare activity, and solar wind streams. The both satellites responded to the CME coming on April 18. This latter became the reason of a minor (minor $K_p = 5,\ G = 1$) sudden geomagnetic storm (that is confirmed by the geomagnetic disturbance data) and the shock wave.

– The B-star change (November 2011) is associated with the CMEs produced by the M-class flare on November 9 and the C-class flare on November 11. The elliptical orbit satellite did not experience any disturbances. The possible reason for this is unknown.

The periodogram analysis made in combination with the analysis of the conditions and parameters of space weather makes it possible to see the general and more detailed pattern of the solar and geomagnetic activity influence on the change in the satellite motion in the atmosphere.

The B-star drag term helps to consider only the atmosphere influence on the satellite movement in the near-Earth space.

## REFERENCES

1. JACCHIA, L. G., SLOWEY, J. W. and CAMPBELL, I. G., 1968. A Study of the Semiannual Density Variation in the Upper Atmosphere from 1958 to 1966, Based on Satellite Drag Analysis. *SAO Spec. Rep.* no. 265.
2. VON ZAHN, U., 1970. Neutral air density and composition at 150 kilometers. *J. Geophys. Res. Space. Phys.* vol. 75, is. 28, 5517–5527. DOI: 10.1029/JA075i028p05517
3. JACCHIA, L. G., 1965. Density Variations in the Heterosphere. *SAO Spec. Rep.* no. 184.
4. HARRIS, I. and PRIESTER, W., 1962. Time-dependent structure of the upper atmosphere. *J. Atmos. Sci.* vol. 19,

no. 4, pp. 286–301. DOI: 10.1175/1520-0469(1962)019<0286:TDSOTU>2.0.CO;2
5. NICOLET, M., 1963. Solar radio flux and temperature of the upper atmosphere. *J. Geophys. Res.* vol. 68, is. 22, pp. 6121–6144. DOI: 10.1029/JZ068i022p06121
6. KING, J. W., ECCLES, D., LEGG, A. J., SMITH, P. A., GALINDO, P. A., KAISER, B. A., PREECE, D. M. and RICE, K. C., 1964. *An Explanation of Various Ionospheric and Atmospheric Phenomena including the Anomalous Behaviour of the F-Region*. Radio Research Station, Ditton Park, Slough, England. Document No. RRS/I.M. 191, December.
7. JACCHIA, L. G., 1967. Recent Results in the Atmospheric Region above 200 km and Comparisons with CIRA 1965. *SAO Spec. Rep.* no. 245.
8. ROEMER, M., 1967. Geomagnetic activity effect and 27–day variation: response time of the thermosphere and lower exosphere. In: R. L. SMITH-ROSE, S. A. BOWHILL, and J. W. KING, eds. *Space Research VII.* Amsterdam: North-Holland Publ. Co., pp. 1091–1099.
9. JACCHIA, L. G., 1967. Properties of the Upper Atmosphere Determined from Satellite Orbits. *Philos. Trans. R. Soc. Lond. A.* vol. 262, no. 1124, pp. 157–171.
10. DOORNBOS, E. and KLINKRAD, H., 2006. Modelling of space weather effects on satellite drag. *Adv. Space Res.* vol. 37, is. 6, pp. 1229–1239. DOI: 10.1016/j.asr.2005.04.097
11. KRASSOVSKY, V. I., 1968. Heating of the Upper Atmosphere during Geomagnetic Disturbances. *Nature*. vol. 217, is. 5134, pp. 1136–1137. DOI: 10.1038/2171136a0
12. COLE, K. D., 1971. Electrodynamic heating and movement of the thermosphere. *Planet. Space Sci.* vol. 19, is. 1, pp. 59–75. DOI: 10.1016/0032-0633(71)90067-5
13. ILLÉS-ALMÁR, E., 2004. Two distinct sources of magnetospheric heating in the atmosphere: the aurora and ring current. *Adv. Space Res.* vol. 34, is. 8, pp. 1773–1778. DOI: 10.1016/j.asr.2003.04.059
14. CROFT, T. A., 1971. Corotating Regions in the Solar Wind, Evident in Number Density Measured by a Radio-Propagation Technique. *Radio Sci.* vol. 6, is. 1, pp. 55–63. DOI: 10.1029/RS006i001p00055
15. SLOWEY, J., 1964. Atmospheric Densities and Temperatures from the Drag Analysis of the Explorer 17 Satellite. *SAO Spec. Rep.* no. 157.
16. JACCHIA, L. G., SLOWEY, J. and VERNIANI, F., 1967. Geomagnetic perturbations and upper-atmosphere heating. *J. Geophys. Res.* vol. 72, is. 5, pp. 1423–1434. DOI: 10.1029/JZ072i005p01423
17. KING-HELE, D. G. and WALKER, D. M. C., 1971. Air density at heights near 180 km in 1968 and 1969, from the orbit of 1967-31a. *Planet. Space Sci.* vol. 19, is. 3, pp. 297–311. DOI: 10.1016/0032-0633(71)90094-8
18. MAY, B. R. and MILLER, D. E., 1971. The correlation between air density and magnetic disturbance deduced from changes of satellite spin-rate. *Planet. Space Sci.* vol. 19, is. 1, pp. 39–48. DOI: 10.1016/0032-0633(71)90065-1
19. SLOWEY, J. W., 1984. *Dynamic model of the Earth's upper atmosphere.* Washington, D.C.: National Aeronautics and Space Administration, Scientific and Technical Information Branch.
20. FRIIS-CHRISTENSEN, E., LASSEN, K., WILHJELM, J., WILCOX, J. M., GONZALEZ, W. and COLBURN, D. S., 1972. Critical component of the interplanetary magnetic field responsible for large geomagnetic effects in the polar cap. *J. Geophys. Res. Space Phys.* vol. 77, is. 19, pp. 3371–3376. DOI: 10.1029/JA077i019p03371
21. BELETSKY, V. V., 1965. *Motion of an Artificial Satellite with Respect to the Center of Mass.* Moscow, Russia: Nauka Publ. (in Russian).
22. ROY, A., 1981. *Orbital motion.* Moscow, Russia: Mir Publ. (in Russian)
23. KELSO, T., 1998. Frequently Asked Questions: Two-Line Element Set Format. *Satellite Times.* vol. 4, no. 3, pp. 52–54.
24. HOOTS, F. R. and ROEHRICH, R. L., 1988. Models for Propagation of NORAD Element Sets. *Spacetrack Report.* no. 3.
25. VALLADO, D. A., CRAWFORD, P., HUJSAK, R. and KELSO, T. S., 2017. Revisiting Spacetrack Report no. 3: Rev2. In: *AIAA/AAS Astrodynamics Specialists Conference and Exhibit.* Keystone, CO: American Institute of Aeronautics and Astronautics, Inc., id. AIAA 2006-6753-Rev2. Available from: http:celestrak.com/publications/AIAA/2006-6753/AIAA-2006-6753-Rev2.pdf
26. NATIONAL OCEANIC AND ATMOSPHERIC ADMINISTRATION. *Catalog of solar activity and space weather – Weekly* [online]. [viewed 18 June 2020]. Available from: ftp://ftp.swpc.noaa.gov/pub/warehouse/2015/WeeklyPDF/

*В. Г. Комендант*

Обсерваторія "УРАН-4", Радіоастрономічний інститут НАН України,
вул. Маразліївська, 1 в, Астрономічна обсерваторія,
м. Одеса, 65014, Україна

## ЩОДО ХАРАКТЕРУ ГАЛЬМУВАННЯ ШТУЧНИХ СУПУТНИКІВ ЗЕМЛІ ЗА РІЗНИХ СТАНІВ СОНЯЧНОЇ Й ГЕОМАГНІТНОЇ АКТИВНОСТІ

*Предмет і мета роботи:* Гальмування штучних супутників Землі в атмосфері залишається актуальною проблемою. З метою дослідження стану атмосфери при різних проявах сонячної та геомагнітної активності в роботі використано дані штучних супутників Землі. Обрані космічні апарати рухалися у некерованому стані і були хорошими індикаторами стану верхніх шарів атмосфери. У роботі використано коефіцієнт гальмування B-star (drag term). Цей коефіцієнт в моделях SGP і SDP служить для врахування опору атмосфери орбітальному руху космічного апарата. Розглянуто дані про гальмування двох штучних супутників Землі, які рухалися один за еліптичною, а другий за круговою орбітою на середніх широтах (нахил орбіт $58° \div 60°$) Досліджуваний інтервал часу включає фазу спаду 23-го циклу сонячної активності та фази зростання, максимуму і спаду 24-го сонячного циклу (2005–2017 рр.). Розглянуто 7 явно виражених періодів гальмування цих супутників – 4 періоди по одному місяцю (два у 2005 р. і два у 2011 р.), і 3 періоди тривалістю в рік (з 19 липня 2014 р. до 22 серпня 2015 р.), в п'ять років (2005–2010 рр.) та шість років (2011–2017 рр.).
*Методи і методологія:* Виконано періодограмний аналіз, що дозволив виявити періодичні процеси в змінах стану ат-

мосфери різної тривалості. Зроблено розрахунки коефіцієнтів кореляції B-star з індексами сонячної та геомагнітної активності. Виконано аналіз екстремальних гальмувань супутників в періоди підвищеної сонячної і геомагнітної активності (інтервали спостережень тривалістю в місяць).

*Результати:* З використанням сонячних і геомагнітних даних було встановлено, що частина аномальних періодів гальмування тривалістю в місяць супроводжувалася спалаховими явищами на Сонці і приходом корональних викидів маси в навколоземний простір. На інтервалах спостережень в один рік найвищі значення $(0.5 \div 0.7)$ були отримані для коефіцієнтів кореляції параметра B-star з індексами сонячної активності: з радіовипромінюванням Сонця на довжині хвилі 10.7 см ($F10.7$) і з випромінюванням Лаймана альфа ($L_\alpha$). На часовому інтервалі спостережень в один місяць найбільші значення отримані для коефіцієнтів кореляції B-star з потоками електронів з енергіями понад 0.6 і 2 МеВ $(0.3 \div 0.5)$, з випромінюванням Лаймана альфа $L_\alpha$ $(0.58 \div 0.73$ для супутника на круговій орбіті), з сонячною сталою *TSI* $(0.3 \div 0.6)$, а також з індексом інтенсивності геомагнітних бур $D_{st}$ $(0.66 \div 0.69)$. Розрахунки періодограмм демонструють присутність цілого спектра періодів в гальмуванні супутника на круговій орбіті і виділеного періоду для супутника на еліптичній орбіті.

*Висновки:* Розглянуто залежності коефіцієнту гальмування B-star від індексів сонячної і геомагнітної активності під час окремих періодів їх посилення протягом 23–24 циклів сонячної активності. Проведений періодограмний аналіз в поєднанні з аналізом умов і параметрів космічної погоди дозволяє побачити загальну і більш детальну картину впливу сонячної і геомагнітної активності на зміну руху штучних супутників Землі в атмосфері. Коефіцієнт B-star допомагає розглядати вплив виключно атмосфери на рух штучних апаратів в навколоземному просторі.

*Ключові слова:* штучні супутники Землі, атмосфера, гальмування штучних супутників Землі, сонячна активність, геомагнітна активність, космічна погода

*Received 19.10.2020*